Landé g_J values in atomic argon: A measurement of the ratio $g_J(2p_9)/g_J(1s_5)$ by saturation spectroscopy

J. R. Brandenberger
Department of Physics, Lawrence University, Appleton, Wisconsin 54912
(Received 11 February 1999; revised manuscript received 22 April 1999)

Saturation spectroscopy capitalizing on the presence of negative crossover signals has been exploited to measure the ratio of two Landé g_J values in atomic argon. The result, $g_J(2p_9)/g_J(1s_5)=0.88845(7)$, leads to a value for $g_J(2p_9)=1.3335(1)$, which is 100 times more certain than its best previous determination but discrepant with existing theoretical values. [S1050-2947(99)03608-2]

PACS number(s): 32.60.+i, 32.80.Bx, 39.30.+w, 42.62.Fi

I. INTRODUCTION

Saturation spectroscopy provides a Doppler-free technique for measuring hyperfine structure, isotope shifts, Stark and Zeeman splittings, and other quantities of interest in atomic and molecular physics [1]. The technique employs tunable laser beams that counterpropagate through a target generating narrow, velocity-selective, saturated-absorption features. This paper reports on the use of saturation spectroscopy to compare the Zeeman structures of the $1s_5$ and $2p_9$ states of argon [2], the objective being to determine the g_J value of the $2p_9$ state. As discussed below, $g_J(2p_9)$ is difficult to measure; its best determination to date is two orders of magnitude less certain than measurements of other g_J values in excited states of Ar. We choose to measure the *ratio* $g_J(2p_9)/g_J(1s_5)$ for two reasons: $g_J(1s_5)$ is already well known, and hence a measurement of the ratio yields an immediate determination of $g_J(2p_9)$; and secondly, measuring $g_J(2p_9)/g_J(1s_5)$ circumvents determination of the magnetic field and lets us exploit a highly redundant Zeeman spectrum to achieve better statistics and explore systematic effects.

The Landé formula for g_J embraces Russell-Saunders coupling but ignores configuration interaction, intermediate coupling, relativistic, QED and other effects [3]. Even so, its predictions are noteworthy: $g_J(1s_5)=1.500$, $g_J(2p_9)=1.333$, and hence $g_J(2p_9)/g_J(1s_5)=0.889$. More sophisticated calculations yielding $g_J(1s_5)=1.50106$ [4], $g_J(2p_9)=1.3341$ [5], and thus $g_J(2p_9)/g_J(1s_5)=0.88877$ deviate comparatively little from the Russell-Saunders values. Experimentally, $g_J(1s_5)$ is well known due to the 5 ppm measurement $g_J(1s_5)=1.500964$ [6], but the best measurement of $g_J(2p_9)$ to date is 1.338, thought to be good to 1% [7]. These values yield the experimental ratio $g_J(2p_9)/g_J(1s_5)=0.891$, also good to 1%. This paper reports an experimental value of $g_J(2p_9)/g_J(1s_5)$ which is two orders of magnitude more certain.

II. EXPERIMENT

The 811.53 mm $1s_5 \Leftrightarrow 2p_9$ transition in Ar provides exclusive access to the $2p_9$ state from below. Unfortunately the Zeeman structure in this line tends to overlap due to the near equality of the $1s_5$ and $2p_9$ g_J values. Hence use of the 811.53 nm line to measure the ratio $g_J(2p_9)/g_J(1s_5)$ requires fairly high resolution. While difficulties with resolution have deterred others [8] from measuring $g_J(2p_9)$, we show below that saturation spectroscopy in this case offers enhanced resolution due to the presence of negative crossover signals. Figure 1 shows the $1s_5$ and $2p_9$ Zeeman sublevels along with transition probabilities and a saturation spectrum that exhibits 27 Zeeman features, some of which are negative crossovers. Since argon is 99.6% ^{40}Ar$(I=0)$, we observe no hyperfine structure.

The experimental layout shown in Fig. 2 includes an external cavity diode laser that generates a linearly-polarized 1 mW pump beam and two 25-μW probe beams, each of nominal intensity 3 μW/mm^2. A Glan-Thompson prism serves as a linear polarizer, and neutral density filters attenuate the beams before they traverse a 2.5 cm diam$\times$10 cm cell containing 300 mTorr of Ar at 296 K. The pump beam de-

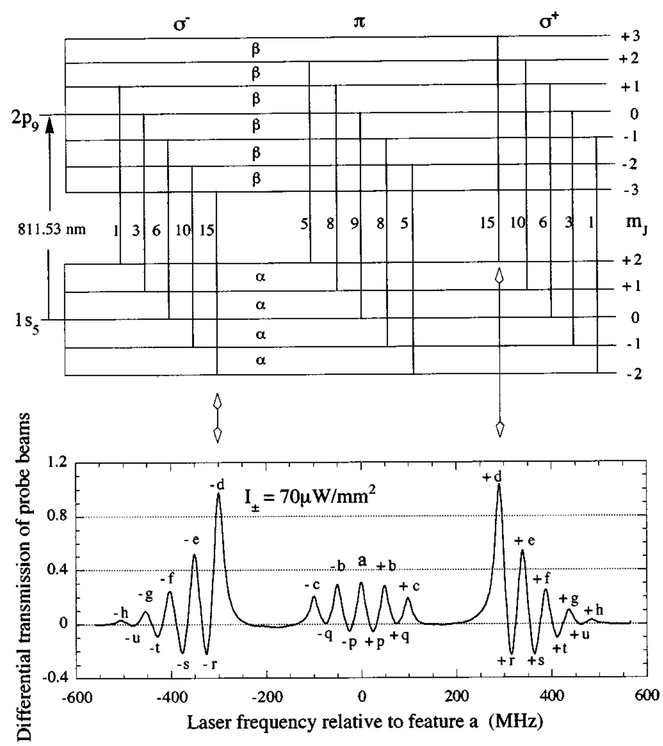

FIG. 1. Zeeman levels, relative transition probabilities, and saturation spectrum for a magnetic field of roughly 200 G. Features $\pm p$ through $\pm u$ are negative crossover signals.

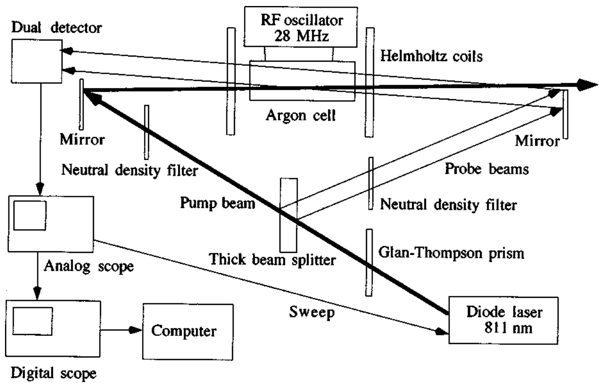

FIG. 2. Experimental layout for measuring g_J values in excited states of argon by saturation spectroscopy.

livers an average intensity of 140 μW/mm^2 [9] to the target where a weak 28 MHz rf-discharge promotes Ar atoms into the $1s_5$ state. Atoms in the $1s_5$ metastable state are excited to the $2p_9$ state by laser light. Helmholtz coils produce a magnetic field of 200 G directed along the optic axis. The detector monitoring the probe beams generates a sufficiently quiet difference signal to obviate chopping of the laser beams. A digital scope captures and averages the spectra.

III. LINE-SHAPE CONSIDERATIONS

We begin by analyzing the effects of laser intensity and atomic branching on the shapes of the Zeeman features. Our purpose is to show that the linewidths and branching ratios comport well with the heights and signs of the various features, thereby suggesting that the saturation spectrum is sufficiently well-understood to warrant careful spectral analysis. The positive features in Fig. 1 are $a, \pm b, \ldots, \pm h$, the negative features $\pm p, \pm q, \ldots, \pm u$. A positive peak signifies increased transmission by the probe beam that passes through an Ar population partially depleted by circularly-polarized pump beams of intensity $I_{\pm}=70\ \mu$W/mm^2 [9]. These strong counterrotating pump beams broaden the peaks to 20 MHz or more FWHM. All peaks share the same low-intensity homogeneous width $\Delta\nu_0=\gamma/2\pi=(1/\tau+2/T_{\rm int})/2\pi$, where $\tau=30.9$ nsec is the $2p_9$ lifetime [10] and $2/T_{\rm int}$ reflects the interaction time $T_{\rm int}=225$ nsec. Hence $\Delta\nu_0=6.56$ MHz, and the total width $\Delta\nu_{\rm total}$ scales with $I_{\pm}$ according to

$$\Delta\nu_{\rm total}=\Delta\nu_0[1+(1+I_{\pm}/I_{\rm sat})^{1/2}]/2+\Delta\nu_{\rm laser}+\Delta\nu_{\rm geom}, \quad (1)$$

where $I_{\rm sat}$ is the saturation intensity, $\Delta\nu_{\rm laser}\approx 1.5$ MHz, and $\Delta\nu_{\rm geom}\approx 4.7$ MHz reflects the angle between pump and probe beams [1]. Equation (1) predicts a low-intensity width $\Delta\nu_{\rm total}=12.8$ MHz, which agrees with our measured values of 13(1) MHz.

Taller and broader than expected, features $\pm d$ stem from two-level cycling transitions $|1s_5 m_J=\pm 2\rangle \Leftrightarrow |2p_9 m_J=\pm 3\rangle$ whose saturation intensities should be $I_{\rm sat}=2\pi hc\gamma/6\lambda^3=16.1\ \mu$W/mm^2 [11]. However, if the experimental $I_{\pm}=70\ \mu$W/mm^2 and $\Delta\nu_{\rm total}(\pm d)=23.4$ MHz [12] are substituted into Eq. (1), one infers a significantly reduced saturation intensity of 4.1 μW/mm^2. We attribute this fourfold reduction in $I_{\rm sat}$ to *collisional disorientation*, which redistributes Ar atoms among various Zeeman levels and combines with spontaneous decay to disrupt the cyclic nature of the $\pm d$ transitions.

Beyond $\tau(2p_9)$ and $T_{\rm excite}\approx\tau(2p_9)$ [13], two other time intervals are relevant. One is the interaction time $T_{\rm int}$ during which atoms resonate with the laser light; velocity-changing collisions initiate and terminate $T_{\rm int}$ via Doppler tuning and detuning. Taking the kinetic cross section to be $\sigma_k\approx 0.8\times 10^{-14}$ cm^2 [14], $n=10^{16}$ atoms/cm^3, and the relative atomic velocity $v_{\rm rel}=5.57\times 10^4$ cm/sec, we find that $T_{\rm int}=(n\sigma_k v_{\rm rel})^{-1}=225$ nsec. In the same way one can invoke the cross section for collisional disorientation, $\sigma_D\approx 2\times 10^{-14}$ cm^2 [15], to calculate the mean time between disorienting collisions $T_D\approx 90$ nsec. These four time intervals imply that an Ar atom resonating on feature $\pm d$ spends about half its time in the $|2p_9 m_J=\pm 3\rangle$ state awaiting a highly-probable disorienting collision, which, with spontaneous decay, tends to eject the atom from the cycle. Pappas *et al.* show that when a cycling transition is disrupted in this way, a *reduced saturation intensity* $I_1=(h\nu/\sigma_0\tau)(1+\tau/T_{\rm int})/(2+\Gamma_1 T_{\rm int})$ becomes the preferred measure of pump intensity [16], where Γ_1 is the decay rate from the upper level to all lower levels *except the original*. Substituting the aforementioned $I_1=4.1\ \mu$W/mm^2 into Pappas' expression yields $\Gamma_1(\pm d)=31$ Mrad/sec, implying that a $|2p_9, m_J=\pm 3\rangle$ Ar atom stands roughly a 70% chance of returning to its original $|1s_5, m_J=\pm 2\rangle$ state [17]. For peaks $\pm e$, $\Delta\nu_{\rm total}(\pm e)=21.7$ MHz, $I_1=5.5\ \mu$W/mm^2, $\Gamma_1=35$ Mrad/sec, and the probability of return becomes about 60%. These probabilities of return are important in what follows.

To analyze the heights of the peaks, we employ Nakayama's approach [18] which uses rate equations to couple as many as four levels in I-, V-, Λ-, and N-type transitions. Given our three-beam layout, the height $h(k)$ of a peak scales as the *difference* in transmission of the two probe beams passing through the target, where one probe beam encounters Ar population that has been pumped. For one cycle of pumping and decay, the relative height [18] is

$$h(k)=|\mu_i|^2|\mu_j|^2[-\delta_{i,sp}+|\mu_{sp}|^2/\Gamma]f_{\rm Dopp}, \quad (2)$$

where the $|\mu_i|^2$ and $|\mu_j|^2$ are pump and probe transition probabilities. Γ is the spontaneous decay rate of the upper level, $f_{\rm Dopp}$ is the relative population of the velocity group being pumped, and $|\mu_{sp}|^2$ is the decay rate from the upper level to the lower level being probed. Thus $|\mu_{sp}|^2/\Gamma$ is the fractional probability that an excited atom decays to the probed level, and $\delta_{i,sp}$ accounts for pumped depletion of the probed level. For I-type features, $\delta_{i,sp}=1$; otherwise $\delta_{i,sp}=0$. For transition d, $|\mu_{sp}|^2/\Gamma\approx 0.7$ and $f_{\rm Dopp}=1$. Thus, $[-\delta_{i,sp}+|\mu_{sp}|^2/\Gamma]=-0.3$, and Eq. (2) predicts a feature height $h(d)=|\mu_i|^2|\mu_j|^2(-0.3)=225(-0.3)=-67.5$, where the sign indicates depletion of the probed level. After normalization to itself, $h(d)$ becomes -1. These and similar calculations appear in Table I. Negative values of $h(k)$ correspond to positive peaks in Fig. 1.

Figure 3 depicts three resonances starting with feature *d*. The bold arrow represents pumping, the faint arrow probing of the $|1s_5 m_J=+2\rangle$ population. As mentioned above, collisional disorientation causes about 30% of the pumped atoms to decay *outward* leaving 70% to return to $|1s_5 m_J=+2\rangle$.

TABLE I. Contributions to the heights of selected features. Successive columns identify the type, initial, and final quantum numbers for pump and probe transitions, products of relevant transition probabilities, fractional probabilities for a pumped atom to return to the probed level, the atomic velocity $v=\lambda\Delta\gamma_{\rm Dopp}$ along the pump beam necessary to shift the laser light by $\Delta\nu_{\rm Dopp}$ to bring it into resonance with the moving atom, and the Doppler population factor $f_{\rm Dopp}=\exp[-(\Delta\omega_{ij}/2ku)^2]$ applicable to crossover resonances, where $u=3.51\times10^4$ cm/sec is the most probable Ar velocity. The total heights $h(k)$ are normalized to feature $+d$ in the eleventh column. The last column contains experimental heights $h_{\rm expt}$ derived from fitting the sum of 27 Lorentzians to the spectrum of Fig. 1. Asterisks identify fractional probabilities that reflect collisional disorientation.

Peak	Type	Pump m	m′	Probe m	m′	$\|\mu_i\|^2\|\mu_j\|^2$	$\|\mu_{\rm sp}\|^2/\Gamma$	$\delta_{i,sp}$	Velocity (10^4 cm/sec)	$f_{\rm Dopp}$	$h(k)$	$h_{\rm norm}$	$h_{\rm expt}$
a	V	0	1	0	−1	6×6	6/15	1	−3.12	0.450	−9.72		
a	V	0	−1	0	1	6×6	6/15	1	3.12	0.450	−9.72		
a	Λ	1	0	−1	0	3×3	3/15	0	−3.52	0.364	0.66		
a	Λ	−1	0	1	0	3×3	3/15	0	3.52	0.364	0.66		
$a_{\rm tot}$											−18.12	−0.27	−0.31
$-b$	V	1	−1	1	2	3×10	3/15	1	3.12	0.450	−10.80		
$-b$	V	1	2	1	−1	10×3	10/15	1	−3.12	0.450	−4.50		
$-b$	Λ	2	1	0	1	1×6	6/15	0	3.52	0.364	0.87		
$-b$	Λ	0	1	2	1	6×1	1/15	0	−3.52	0.364	0.15		
$-b_{\rm tot}$											−14.28	−0.21	−0.28
$+d_{\rm tot}$	I	2	3	2	3	15×15	0.70*	1	0	1	−67.50	−1.00	−1.00
$+e_{\rm tot}$	I	1	2	1	2	10×10	0.60*	1	0	1	−40.00	−0.59	−0.55
$+f_{\rm tot}$	I	0	1	0	1	6×6	0.55*	1	0	1	−16.20	−0.26	−0.27
$+g_{\rm tot}$	I	−1	0	−1	0	3×3	3/15	1	0	1	−7.20	−0.11	−0.11
$+h_{\rm tot}$	I	−2	−1	−2	−1	1×1	1/15	1	0	1	−0.93	−0.01	−0.04
$-p$	N	1	0	0	1	3×6	9/15	0	−3.32	0.406	4.38		
$-p$	N	0	1	1	0	6×3	8/15	0	3.32	0.406	3.90		
$-p_{\rm tot}$											8.28	0.12	0.11
$-r_{\rm tot}$	N	−1	−2	−2	−3	10×15	0.20*	0	0.20	0.997	29.91	0.44	0.44

This 0.7 fractional probability of return largely explains why peaks $\pm d$ are so tall: absent disorientations, the probability of return would be unity, and $h(d)$ would be zero. Figure 3 also depicts feature $-r$, a crossover for which pumping and probing involve different Zeeman pairs connected by spontaneous decay. The dashed line represents the laser frequency that lies *midway* between pump and probe frequencies. Axial motion by the atoms tunes all three laser beams into simultaneous resonance with the two transitions. Spontaneous decay in this case *enhances* the $|1s_5m_J=-2\rangle$ population being probed, which explains why peak $-r$ is positive in Table I.

As a final example, consider the V- and Λ-type contributions to feature a in Fig. 3. The dashed lines indicate that the laser is resonant with the $|1s_5m_J=0\rangle\Leftrightarrow|2p_9m_J=0\rangle$ transition. However, since $\sigma^\pm$ laser light cannot drive this transition, this feature must be a crossover resonance. The leftmost V in the diagram represents pumping and probing of $|1s_5m_J=0\rangle$ atoms moving toward the pump beam; 40% of these atoms decay to their original level to be probed. The second V and associated decay are similar except that here the atoms move parallel to the pump beam. In both cases, depopulation of the original state makes the saturation signals negative. Feature a also includes Λ-type contributions whose structures are indicated in the figure and tabulated in Table I. Comparison of the calculated and experimental heights in the last two columns reveals agreement to 20% or better in all but one case. We thereby claim that the spectrum of Fig. 1 is sufficiently well-understood to warrant careful spectral analysis.

Regarding resolutions, we point out that the crossovers $\pm r$, $\pm s$, $\pm t$, and $\pm u$, situated as they are between pairs of I-type resonances, can enhance or degrade spectral resolution depending upon the signs of their amplitudes. Fortunately in the present work, the amplitudes of these crossovers are negative. It follows that these crossover signals improve our spectral resolution through an approximate tenfold increase in the modulation depth of the spectrum.

IV. SPECTRAL ANALYSIS AND RESULTS

Next we discuss the determination of $g_J(2p_9)/g_J(1s_5)=\beta/\alpha$, where α and β represent the separations between adjacent $1s_5$ and $2p_9$ Zeeman sublevels at fields near 200 G [19]. Our spectra consist of 1000 pairs (s_i,t_i), where s_i represents the *difference* in power between the two probe beams arriving at the detector at time t_i. The center of each feature k lies at a frequency ν_k relative to peak a. Our method of analysis employs six interpeak separations ν_b,ν_c,ν_d,ν_e, $\nu_f=\beta$ and $\nu_g=\alpha$. By defining $\rho=1-\beta/\alpha$, the ratios of these separations can be written $\nu_b/\nu_g=\rho$, $\nu_c/\nu_g=2\rho$, $\nu_d/\nu_g=1-3\rho$, $\nu_e/\nu_g=1-2\rho$, $\nu_f/\nu_g=1-\rho$, and $\nu_g/\nu_g=1$. After manually determining the 13 values of t_k that correspond to the centers of the positive peaks, we offset all

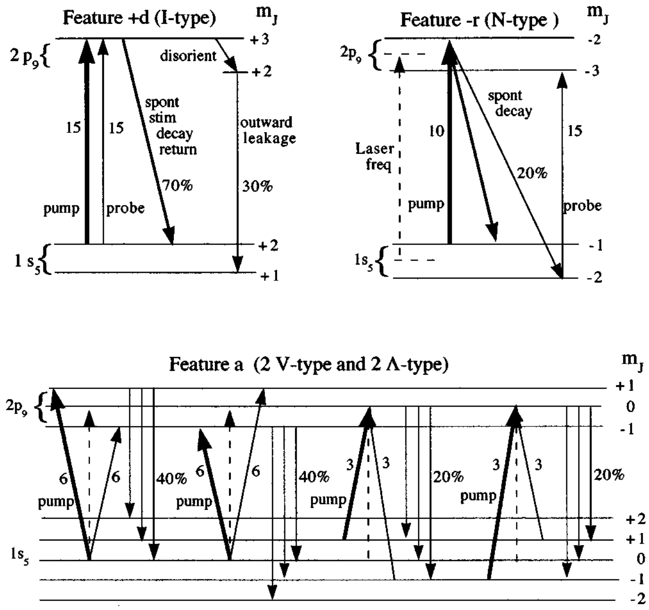

FIG. 3. Saturation features $+d$, $-r$, and a, showing pump and probe transitions (up arrows) and spontaneous decay (down arrows). The diagram illustrates all four types of Nakayama's resonances.

t_k by the same amount to force $t_a=0$. Since our laser scan is slightly nonlinear in time, we express the resonant laser frequencies $\nu_k(t_k)$ in the form $\nu_k(t_k)=Bt_k+Ct_k^2$, where C is presumed small. Dividing this expression by ν_g and redefining constants B and C, we get

$$Bt_b+Ct_b^2=\rho,\quad Bt_c+Ct_c^2=2\rho,\quad Bt_d+Ct_d^2=1-3\rho,$$
$$Bt_e+Ct_e^2=1-2\rho,\quad Bt_f+Ct_f^2=1-\rho,\quad Bt_g+Ct_g^2=1. \tag{3}$$

Substitution of the known t_b through t_g into Eqs. (3) yields six equations which, after elimination of ρ between pairs of them, overdetermine B and C several fold. We proceed to determine the best single value of (B,C) and substitute it back into Eqs. (3) to solve for five values of ρ for each half of a spectrum.

Ten complete spectra similar to the one shown in Fig. 1 have been processed in this manner. Ninety separate values of $\beta/\alpha=1-\rho$ have been determined, each being corrected for "pulling" as described below. The average of these corrected values is $g_J(2p_9)/g_J(1s_5)=\beta/\alpha=0.88845$, with a sample standard deviation of 0.00043 and a standard error of 0.00005 at the 1σ level. Since the total systematic uncertainty is 0.00003 (see next paragraph), the total uncertainty is 0.00007. Hence our final result is $g_J(2p_9)/g_J(1s_5)=0.88845(7)$, which represents an 80 ppm determination, 100 times more certain than the value 0.891 quoted above. Using $g_J(1s_5)=1.500964(8)$, we arrive at our second final result $g_J(2p_9)=1.3335(1)$, also good to 80 ppm and 100 times more certain than the long-standing value 1.338(13) by Green [7].

Three types of systematic error are largely avoided by this method of analysis. The first involves the nonlinearity of the scan. By using six peaks per half spectrum and forcing equality upon their spacings, we measure the nonlinearity and incorporate it into our analysis. The overdetermination of $(B,C)\approx(0.25,10^{-3})$ yields uncertainties $\delta B\approx 10^{-4}$ and $\delta C\approx 10^{-4}$, whose smallness along with that of C assure that $\nu_k(t_k)=Bt_k+Ct_k^2$ is well-determined. That Ct_k^2 is always less than 1% of $\nu_k(t_k)$ confirms the smallness of the nonlinearity and explains our omission of higher order terms in $\nu_k(t_k)$. We also derive assurance from the fact that the values of (B,C) change very little from one half-spectrum to another. We estimate that any residual systematic effect due to scan nonlinearity should contribute no more than 15 ppm to the value of β/α. A second possible systematic error involves the "pulling" of the centers of the positive peaks due to encroachment by neighboring negative features. Such encroachment pushes peaks $\pm b$ and $\pm c$ *away* from the central peak because of the unequal heights of negative features $\pm p$ and $\pm q$. Peaks $\pm d$, on the other hand, are pulled *toward* the central peak because of the unbalanced presence of features $\pm r$. To correct for these effects, we perform line shape simulations to infer the amount of pulling of the center frequencies of features $\pm b$ through $\pm f$ due to negative crossovers. These simulations produce factors that let us correct the $(\beta/\alpha)_k$ [20]. While the individual corrections for each $(\beta/\alpha)_k$ are significant, the *net* correction of the grand average $\beta/\alpha=g_j(2p_9)/g_J(1s_5)$ amounts to less than 20 ppm, which we take to be the residual systematic uncertainty due to pulling.

A third possible source of systematic error involves magnetic field inhomogeneity, which is about 0.01% in our interaction region. Another round of simulations, this time field dependent, confirms that the experimental determination of β/α is very insensitive to changes in the field or to the existence of field inhomogeneity; any systematic effect of this sort should affect β/α by less than 10 ppm. Combining these three estimates of systematic error in quadrature, we get a total systematic uncertainty of 0.00003 in 0.88845.

V. DISCUSSION

The theoretical counterpart $g_{\gamma J}$ to our experimental result $g_J(2p_9)=1.3335(1)$ is given by the expression [3]

$$g_{\gamma J}=\sum_{\alpha LS}\langle\gamma J|\alpha LSJ\rangle^2 g_{LSJ}, \tag{4}$$

where, in our case, the sum is confined strictly to terms with $J=3$ and even parity since our primary base state $|2p_9\rangle=|3p^5 4p[5/2]_{J=3}\rangle$ has even parity. Since the $|2p_9\rangle$ state is the only $J=3$ state in the $3p^5 4p$ configuration, intermediate coupling within this configuration is completely absent, and the LS specification $4p\ {}^3D_3$ is highly appropriate. A latter-day version of the Landé formula assumes the form [3]

$$g_{LSJ}=g_L+(g_s-1)[J(J+1)+S(S+1)-L(L+1)]/2J(J+1), \tag{5}$$

where $g_L=(1-m_e/40M_p)=0.999986$ and $g_s=2.002319$. This expression yields $g_{LSJ}=g_{213}=1.3341$, which receives a very high degree of weighting in the sum Eq. (4) since the closest even-parity $J=3$ neighbor is the state $|3p^5 5p[5/2]_{J=3}\rangle$ which lies 11480 cm^{-1} higher. This latter state also exhibits a high degree of ${}^3D_3$ character, implying that its g_{LSJ} is also about 1.334. Thus the convergence of the weighted sum in Eq. (4) towards $g_{\gamma J}=1.3341$ is very strong. It follows that configuration interaction offers little prospect for resolving the 400 ppm discrepancy between our experimental $g_J(2p_9)=1.3335(1)$ and the prediction of $g_{\gamma J}=1.3341$.

It is beyond the level of this paper to pursue this discussion further except to point out that experimental g_J values in the alkalis are known to increase by about 100 ppm with increasing atomic mass. Perl has explored whether this effect might be due to relativistic spin effects [4]. We hope that the present work stimulates new calculations of $g_J(2p_9)$ while we pursue similar measurements of $g(2p_9)$ in neon and krypton.

ACKNOWLEDGMENTS

The author is pleased to acknowledge the contributions of J. M. Reeves and T. W. Beck to this investigation. This work was supported by Research Corporation and Lawrence University.

[1] V. S. Letokhov and V. P. Chebotayev, *Nonlinear Laser Spectroscopy* (Springer-Verlag, Berlin, 1977); see also V. S. Letokhov, in *Saturation Spectroscopy*, edited by K. Shimoda, Topics in Applied Physics Vol. 13 (Springer-Verlag, Berlin, 1976).

[2] For brevity we use Paschen notation: $|1s_5\rangle\approx|4s\ {}^3P_2\rangle\approx|3p^54s[3/2]_{J=2}\rangle$ and $|2p_9\rangle\approx|4p\ {}^3D_3\rangle\approx|3p^54p[5/2]_{J=3}\rangle$.

[3] R. D. Cowan, *The Theory of Atomic Structure and Spectra* (University of California Press, Berkeley, 1981), pp. 485–497.

[4] A. Lurio, C. Drake, V. W. Hughes, and J. A. White, Bull. Am. Phys. Soc. **3**, 8 (1958); see also W. Perl, Phys. Rev. **91**, 852 (1953); A. Abragam and J. H. Van Vleck, *ibid.* **92**, 1448 (1953).

[5] See Sec. V for a discussion of this value.

[6] A. Lurio, C. Drake, V. W. Hughes, and J. A. White, Bull. Am. Phys. Soc. **3**, 8 (1958). H. Abu-Safia *et al.* report a 130 ppm value for $g_J(1s_5)=1.5008$; see H. Abu-Safia, J. P. Grandin, and X. Husson, J. Phys. B **14**, 3363 (1981).

[7] J. B. Green and B. Fried, Phys. Rev. **54**, 876 (1938); C. E. Moore, *Atomic Energy Levels*, NSRDS-NBS 35 (revised) (U.S. GPO, Washington, DC, 1971), Vol. I.

[8] H. Abu-Safia, J. P. Grandin, and X. Husson, J. Phys. B **14**, 3363 (1981); H. Abu-Safia and J. Margerie, *ibid.* **16**, 927 (1983).

[9] High pump intensities are required here to render all 27 features observable in a single spectrum. The $I_{\rm tot}=140\ \mu$W/mm^2 of linearly-polarized pump intensity and its counterrotating components $I_{\pm}=70\ \mu$W/mm^2 represent intensities averaged over Gaussian pump and probe profiles. A simpler average of $I_{\pm}=50\ \mu$W/mm^2 is based upon a total pump power of 800 μW and an elliptically shaped beam spot of area 8(1) mm^2 chosen at the $1/e^2$ points.

[10] This 30.9(1) nsec lifetime represents an average of several experimental values. See M. J. G. Borge and J. Campos, J. Quant. Spectrosc. Radiat. Transf. **24**, 263 (1980); D. A. Landman, Phys. Rev. **173**, 33 (1968).

[11] This expression combines the two-level definition $I_{\rm sat}=h\nu/2\sigma_0\tau$ with $\sigma_0=16\pi^2k|\mu_{ij}|^2/h\gamma$ and $|\mu_{ij}|^2=3hc^3/8\pi\omega^3\tau$. See P. G. Pappas *et al.*, Phys. Rev. A **21**, 1955 (1980); A. Corney, *Atomic and Laser Spectroscopy* (Clarendon Press, Oxford, 1977), p. 99.

[12] Experimental linewidths $\Delta\nu_{\rm tot}$ are determined by fitting a sum of 14 independently adjustable Lorentzians to one-half of the spectrum of Fig. 1.

[13] For a two-level cycling transition driven at an intensity $I_{\pm}=2I_{\rm sat}$, the mean excitation time is $T_{\rm excite}\approx\tau(2p_9)$.

[14] D. A. Landman, Phys. Rev. **173**, 33 (1968).

[15] This estimate of σ_D is based upon the measured cross section for collisional disalignment $\sigma_2=2.14\times10^{-14}\,{\rm cm}^2$ for $2p_9$ Ar atoms moving among ground state Ar atoms. See D. A. Landman, Phys. Rev. **173**, 33 (1968).

[16] P. G. Pappas *et al.*, Phys. Rev. A **21**, 1955 (1980).

[17] This figure of 70% stems from the following: the spontaneous decay rate is $\Gamma_{\rm spon}(2p_9)\approx32$ Mrad/sec, and the collisionally induced decay rate is $2/T_{\rm int}(2p_9)\approx9$ Mrad/sec. With $I_{\pm}\approx4I_{\rm sat}$, it follows that $\Gamma_{\rm stim}\approx2\Gamma_{\rm spon}\approx64$ Mrad/sec. Thus the total relaxation rate from the $|2p_9m_J=\pm3\rangle$ state is about 105 Mrad/sec. With $\Gamma_1=31$ Mrad/sec, the probability for outward decay becomes $31/105\approx0.3$. Hence the probability for return to the $|1s_5m_J=\pm2\rangle$ state is roughly 0.7.

[18] S. Nakayama, Phys. Scr. **T70**, 64 (1997). Although Nakayama's formalism assumes weak pumping, we invoke it anyway because of its simplicity and its past success in dealing with cases of moderately high pumping intensity. See S. Nakayama, G. W. Series, and W. Gawlik, Opt. Commun. **34**, 382 (1980).

[19] The use of α and β in this way is tantamount to assuming that the quadratic Zeeman effect is negligible for these states in these fields. This assumption is valid since Zeeman curvature scales as $(g_J\mu_0B/\Delta E_{J=3})^2\approx10^{-12}$.

[20] The corrections for $(\alpha/\beta)_k$ are $+85$, $+20$, $+170$, -20, and -265 ppm, respectively, for peaks $\pm b$ through $\pm f$. Hence the *net* correction to overcome pulling for an evenly weighted ensemble of the five features is less than 20 ppm.